

NACA RM L53F19a

UNCLASSIFIED

# NACA

## RESEARCH MEMORANDUM

A ROCKET-MODEL INVESTIGATION OF THE  
LONGITUDINAL STABILITY, LIFT, AND DRAG CHARACTERISTICS  
OF THE DOUGLAS X-3 CONFIGURATION WITH HORIZONTAL  
TAIL OF ASPECT RATIO 4.33

By Robert F. Peck and James A. Hollinger

Langley Aeronautical Laboratory  
Langley Field, Va.

CLASSIFIED DOCUMENT

This material contains information affecting the National Defense of the United States within the meaning of the espionage laws, Title 18, U.S.C., Secs. 793 and 794, the transmission or revelation of which in any manner to an unauthorized person is prohibited by law.

### NATIONAL ADVISORY COMMITTEE FOR AERONAUTICS

WASHINGTON  
August 21, 1953

CLASSIFICATION CHANGED

UNCLASSIFIED

*Handwritten:* NACA  
of RA 129 Affection Date 2/11/58  
1954

## NATIONAL ADVISORY COMMITTEE FOR AERONAUTICS

## RESEARCH MEMORANDUM

A ROCKET-MODEL INVESTIGATION OF THE  
LONGITUDINAL STABILITY, LIFT, AND DRAG CHARACTERISTICS  
OF THE DOUGLAS X-3 CONFIGURATION WITH HORIZONTAL  
TAIL OF ASPECT RATIO 4.33

By Robert F. Peck and James A. Hollinger

## SUMMARY

A rocket-propelled model of the Douglas X-3 airplane with an enlarged all-movable horizontal tail of aspect ratio 4.33 has been flown, primarily to determine the effects of the enlarged tail on longitudinal stability, lift, and drag characteristics at transonic and low supersonic speeds. Comparisons made with previously tested models with tails of aspect ratio 3.0 indicate, in general, increases in stability, drag, lift-curve slope, and damping due to enlarging the tail. Rocket-propelled-model data show good agreement with wind-tunnel data.

Data were also obtained on the drag of a model (with a body of revolution) having the same longitudinal distribution of cross-sectional area as the scale airplane model. The transonic drag rise from the two models show agreement within approximately 10 percent.

## INTRODUCTION

Rocket-propelled models are being used by the Langley Pilotless Aircraft Research Division to investigate the longitudinal stability, lift, and drag characteristics of the Douglas X-3 airplane. Two 0.16-scale models of this airplane equipped with all-movable horizontal tail surfaces of aspect ratio 3.0 have been flown, and the resulting data have been presented in references 1 and 2. This paper contains data obtained from the flight of a similar model with a horizontal tail of aspect ratio 4.33 and 39 percent more area, and some effects of the change in tail configuration are shown through comparisons with the data shown in the aforementioned references.

As in previous tests, longitudinal aerodynamic characteristics were obtained from measurements made during the free pitching oscillations following abrupt changes in incidence of the horizontal tail. Data were obtained between Reynolds numbers of  $4 \times 10^6$  and  $12 \times 10^6$  and Mach numbers of 0.6 and 1.43.

A finned body of revolution having the same longitudinal distribution of cross-sectional area as the Douglas X-3 airplane model was also flight tested (fired from helium gun). This was done in connection with a program to check the validity of the transonic drag-rise rule of reference 3 and the resultant data are shown herein. Results of similar tests on another airplane configuration are presented in reference 4.

The models were flown at the Langley Pilotless Aircraft Research Station at Wallops Island, Va.

#### SYMBOLS

$C_L$	lift coefficient, $C_N \cos \alpha - C_C \sin \alpha$
$C_D$	drag coefficient, $C_C \cos \alpha + C_N \sin \alpha$
$C_N$	normal-force coefficient, $\frac{a_n}{g} \frac{W}{Sq}$
$C_C$	chord-force coefficient, $-\frac{a_l}{g} \frac{W}{Sq}$
$C_Y$	side-force coefficient, $\frac{a_t}{g} \frac{W}{Sq}$
$C_m$	pitching-moment coefficient, referenced to 5 percent $\bar{c}$
$P$	period of pitch oscillation, sec
$a_n/g$	normal accelerometer reading, in g units
$a_l/g$	longitudinal accelerometer reading, in g units
$a_t/g$	transverse accelerometer reading, in g units
$W$	weight, lb

S wing area (including area enclosed within fuselage), sq ft  
 A cross-sectional area, sq ft  
 X distance along fuselage (from nose), ft  
 l length of fuselage, ft

$$r_{eq} = \sqrt{\frac{A}{\pi}}, \text{ ft}$$

$$d_{max} = 2(r_{eq_{max}})$$

q dynamic pressure, lb/sq ft  
 $\alpha$  angle of attack, deg  
 $\theta$  angle of pitch, deg  
 R Reynolds number based on wing mean aerodynamic chord  
 M Mach number  
 $\delta$  horizontal-tail deflection, deg  
 t time, sec  
 $T_{1/2}$  time to damp to one-half amplitude, sec  
 $\bar{c}$  wing mean aerodynamic chord, ft  
 V velocity, ft/sec  
 $\Delta p/q$  base pressure coefficient,  $\frac{P_b - P_o}{q}$   
 $P_b$  static pressure measured on base at duct exit station, lb/sq ft  
 $P_o$  free-stream static pressure, lb/sq ft

Subscripts:

$$\dot{\alpha} \quad \frac{1}{57.3} \frac{d\alpha}{dt} \frac{\bar{c}}{2V} \text{ per radian}$$

$$q \quad \frac{1}{57.3} \frac{d\theta}{dt} \frac{\bar{c}}{2V} \text{ per radian}$$

The symbols  $\alpha$ ,  $\dot{\alpha}$ , and  $q$  used as subscripts indicate the derivative of the quantity with respect to the subscripts; for example,

$$C_{L\alpha} = \frac{\partial C_L}{\partial \alpha}.$$

#### MODEL AND APPARATUS

The X-3 configuration tested was the same as that used in tests of references 1 and 2, with the exception of the horizontal tail. The horizontal tail used in this test had approximately 39 percent greater area than the small tail of reference 2 and had an aspect ratio of 4.33 as compared with 3.0 for the small tail. A sketch of the 0.16-scale model is shown in figure 1(a). Use of the bent angle-of-attack-indicator sting provided means of measuring angle of attack up to  $25^\circ$  with a standard indicator which had a range of  $\pm 15^\circ$  relative to the sting.

The model, structurally the same as the models of references 1 and 2, was of all-metal construction. The body was made of magnesium castings and duralumin sheet and the wing and tail surfaces were of solid duralumin. The wing and vertical tail were 4.5 percent thick and the horizontal tail was 5.0 percent thick. All surfaces had a hexagonal airfoil section modified by rounding the corners with a large-radius curvature (a sketch of the airfoil sections is given in refs. 1 and 2).

As in the previous tests, a simple air-induction system in the model was designed to give a mass-flow ratio of about 0.8 through the inlets. These inlets were connected to constant-diameter ducts designed for choked flow at the exits.

A hydraulic accumulator provided power to pulse the horizontal tail in an approximate square wave pattern between deflections of approximately  $-1.25^\circ$  and  $-2.80^\circ$  during the coasting part of the flight. An NACA telemetering system provided continuous information on normal and transverse accelerations in the nose, normal, transverse, and longitudinal accelerations near the center of gravity, angle of attack, control position, free-stream total pressure, calibrated static pressure (measured at base of angle-of-attack indicator), and intermittent measurements of base pressures at two points at the duct exit station. The Doppler velocimeter, NACA modified SCR 584 tracking radar, and radio-sonde were used to check free-stream conditions at the model during the flight.

The weight of the model was 160.3 pounds; the center of gravity was 5.0 percent rearward of the leading edge of the wing mean aerodynamic chord. The moments of inertia of this model in pitch, yaw, and roll were 17.78, 18.09, and 1.4 slug feet<sup>2</sup>, respectively.

The model shown in figure 1(b) has the same longitudinal cross-sectional area distribution as the 0.16-scale rocket model previously described. A breakdown of the rocket-model area distribution and a sketch of an equivalent body of revolution are shown in figure 2.

Photographs of the rocket model and the area-distribution model are shown in figures 3(a) and 3(b), respectively.

### TESTS AND ANALYSIS

The model, which had no sustainer rocket, was propelled to a maximum Mach number of approximately 1.5 by a double ABL Deacon rocket booster from which it separated at rocket burnout. As the model decelerated through the Mach number range it was disturbed in pitch by means of an all-movable horizontal tail. Response of the model to the disturbances was measured by instruments in the model and was transmitted to the ground by means of a telemeter.

During the coasting flight, telemetered information was obtained from which time histories of Mach number, velocity, dynamic pressure, Reynolds number, lift coefficient, drag coefficient, angle of attack, control position, periods of the oscillations due to control disturbance and time for the oscillation to damp to one-half amplitude were obtained. These data were then analyzed by the methods discussed in reference 5 to obtain the variation with Mach number of longitudinal stability, lift, and drag of the configuration. The Reynolds numbers of the test (based on wing mean aerodynamic chord) are shown in figure 4.

During a small portion of the flight of this model a severe vibration was indicated by the two normal accelerometers and the control-position indicator. Since vibration test data obtained before the flight were not sufficient to indicate clearly the cause of this vibration, some additional vibration tests were made on an identical model. A variable-frequency electromagnetic shaker was used to excite the model at its center of gravity. Strain gages mounted in the model, one to indicate bending in the control push rod (which provided linkage between the horizontal tail and the servo mechanism mounted just forward of the duct exit station) and two on the horizontal tail to indicate bending and torsion stresses, provided a measure of the response of these components to the frequencies covered. The type of response of the model components was determined by tactile and visual observation, while records of the stresses in the instrumented components and the shaker calibration indicated the frequency. Response frequencies of some of the important components as determined by these methods were as follows:

Component	Type of response	Frequency, cps
Wing	First bending	93
Wing	Torsion	285
Control push rod	First bending	116
Horizontal tail	First bending	94
Horizontal tail	A combination bending and torsion	116
Horizontal tail	Torsion	550
Tail boom	First bending	130
Fuselage nose	First bending	65

The area-distribution model was fired from a helium gun at Wallops Island and drag data were obtained by means of a Doppler radar unit. The test technique is described in reference 6. The length of the helium-gun model was 1/8 the length of the rocket-propelled model. Reynolds numbers of the helium-gun-model test (shown in fig. 4) are based on a scaled-down wing mean aerodynamic chord which is, of course, 1/8 of the wing mean aerodynamic chord of the rocket model.

#### ACCURACY AND CORRECTIONS

From a consideration of possible zero shifts in the telemetered data of 1 to 2 percent of full-scale instrument range and on the basis of limited checks of Mach number and static pressure, the limits of accuracy of some of the important quantities obtained from the flight test are believed to be as follows:

Mach number	$C_L$	$C_{Dmin}$	$\alpha$ , deg	$\delta$ , deg	M
1.4	$\pm 0.012$	$\pm 0.0010$	$\pm 0.5$	$\pm 0.15$	$\pm 0.01$
1.2	$\pm 0.016$	$\pm 0.0012$	$\pm 0.5$	$\pm 0.15$	$\pm 0.01$
1.00	$\pm 0.022$	$\pm 0.0017$	$\pm 0.5$	$\pm 0.15$	$\pm 0.01$
.85	$\pm 0.032$	$\pm 0.0025$	$\pm 0.5$	$\pm 0.15$	$\pm 0.02$
.7	$\pm 0.050$	$\pm 0.0038$	$\pm 0.5$	$\pm 0.15$	$\pm 0.02$

In addition, the absolute angle of attack may be further in error because of undetermined aerodynamic asymmetry of the free-floating vane used to measure angle of attack. These asymmetry effects may or may not compensate for the possible error of  $\pm 0.5^\circ$  in angle of attack listed previously.

The errors listed as possible in  $C_L$  and  $\alpha$  affect only the absolute level of a particular curve. The deviation of individual points from a straight line is considerably less, resulting in better accuracy on both the trends indicated and on slopes and incremental quantities derived from the measurements.

The indicated angle of attack was corrected for position error due to flight-path curvature and rate of pitch by the method described in reference 7.

None of the accelerometers could be mounted exactly at the center of gravity; therefore, these instruments were affected by angular as well as translatory accelerations of the model. In order to obtain the data presented herein, it was necessary to apply position-error corrections to these instruments to obtain accelerations at the model center of gravity. The nose accelerometers in this model provided data which, when used in conjunction with the measurements made by accelerometers near the center of gravity, described the model motions sufficiently well to provide accelerometer-position-error corrections for all motions except roll acceleration. The model experienced no lateral motions except during a small portion of flight immediately after separation (as indicated by the lateral accelerometers). The roll accelerations during this maneuver were estimated and were found to have no appreciable roll acceleration effects on the accelerometer data as used.

## RESULTS AND DISCUSSION

### General Description of Rocket-Model Flight

A rather violent yaw disturbance resulted from model-booster separation (maximum angle of yaw estimated as approximately  $2^\circ$ ). The subsequent lateral oscillation did not damp out until the model had completed its first two longitudinal oscillations. A time history of  $C_L$  and  $C_y$  during the lateral oscillation is shown in figure 5 to provide a qualitative picture of the model maneuver. This time history starts at 3.5 seconds after take-off at which time the model was definitely ahead of the booster (according to tracking camera records). The first  $C_L$  oscillation (the  $\alpha$  oscillation was qualitatively the same) shown in figure 5 is definitely not the type associated with pure pitch oscillations obtained in tests of this type. An attempt was made to correct the value of  $C_L$  during the first pitch oscillation (between 3.5 and 4.3 seconds) for angle-of-yaw effects through the use of data of reference 8; however, the pitch oscillation showed almost exactly the same rather unusual characteristics after this was done. Longitudinal stability and lift parameter points obtained from the oscillation by the methods of reference 5 show an unusual amount

of scatter, as might be expected, and should be used with caution. This effect has been noted on other configurations at subsonic speeds (refs. 9 and 10). It is believed to result from dynamic coupling (between lateral and longitudinal motions) which precludes successful analysis of the data by linearized procedures.

When the tail pulsed to the  $-1.25^\circ$  position at 4.3 seconds after rocket firing, a very violent vibration (frequency of approx. 105 cps) was indicated primarily by the two normal accelerometers and the control-position indicator. The portion of telemeter record obtained during this vibration is shown in figure 6. The vibration diminished when the tail returned to the  $-2.80^\circ$  position and did not reoccur during the flight. Because these vibrations were obtained during flight, vibration tests were later made on an identical model. These tests which are briefly described in the section entitled "Tests and Analysis" indicated that the flight vibration was of frequency between the first bending frequency of the horizontal tail (98 cps) and an effective torsion frequency of the tail (between 116 and 130 cps). The effective-tail torsion frequency, which is much lower than the torsion frequency of the tail panel itself (550 cps) resulted either from excitation caused by bending of the control-system push rod or by the tail-boom bending. As a result of these tests, it is thought that the phenomenon experienced in flight was tail flutter. Since the model and full-scale airplane are not the same with respect to internal control system and tail-boom structure, the affliction experienced by the model may not be shared by the airplane.

Calculations indicate that during this vibration the model center of gravity moved up and down approximately  $\pm 0.005$  inch and the nose approximately  $\pm 0.012$  inch. The control-position indicator was connected to the control push rod in such a manner that it was actuated by both push-rod bending and control movement. It is believed that only about 20 percent of the  $\pm 0.4^\circ$  amplitude indicated by the control-position indicator resulted from actual tail rotation. This opinion is based to a large extent on observations of the tail action during the vibration tests.

An attempt was made to obtain lift data from the pitch oscillation during flutter by obtaining a mean value from the record. This basically inaccurate procedure resulted in lift data (and, therefore, aerodynamic-center data) of somewhat questionable reliability. The angle-of-attack indicator, however, showed only a small amplitude vibration and, therefore, provided pitch period and time-to-damp information during the flutter.

Subsequent model oscillations during the flight were of a more normal character.

At Mach numbers below approximately 0.86, this model, the small-tail X-3 model, and other models with the X-3 wing in reference 11 were subject to buffet at angles of attack above  $7\frac{1}{2}^{\circ}$  to  $9^{\circ}$ . This was indicated by irregular shaking indicated by the normal-accelerometer records. A portion of record obtained during buffeting is shown in figure 7 along with a portion of record obtained when there was no buffeting. Approximate buffet boundaries determined from the present test are shown in figure 8.

#### Trim

As the horizontal tail was pulsed in coasting flight the model oscillated about trim angle-of-attack and lift-coefficient values shown in figures 8(a) and (b), respectively. The heavy dashes indicate where trim information was actually obtained. The fairing shown for the trim curves for  $\delta = -1.25^{\circ}$  between Mach numbers of 0.9 and 1.0 may be in question because there were not sufficient data to indicate whether there was a "bucket" similar to that shown in the trim curve for  $\delta = -2.80^{\circ}$  between these Mach numbers.

Definite changes in trim with Mach number are indicated by these curves, but when compared with the level-flight trim lift curve for the airplane at 40,000 feet altitude and a wing loading of 120 pounds per square foot (a possible operating condition) the trim changes do not appear serious. This was also true of the small-tail-model trim data given in reference 2.

#### Lift

The basic lift data are given in figure 9 in the form of lift coefficient plotted against angle of attack from each of the model oscillations between Mach numbers of approximately 1.4 and 0.6. In general, the points were obtained over  $1\frac{1}{2}$  cycles of each oscillation. The Mach number variation during the time interval over which the points in this plot were obtained was the order of 0.02 to 0.04, and the average Mach number for each interval is given in the figure. The hysteresis indicated by plots for Mach numbers of 0.83, 0.75, and 0.67 is typical of that obtained from this type test when the model oscillates to lift coefficients near the stall.

The lift-curve slope at trim as obtained from plots such as those given in figure 9 is presented in figure 10 along with the average lift-curve slope of the small-tail X-3 rocket models. In general, the large-tail configuration was indicated to have a slightly higher lift-curve

slope. The lift-curve slope points at Mach numbers of approximately 1.41 and 1.25 are not considered reliable as an indication of pure longitudinal characteristics because of lateral maneuver and flutter effects on measurement of data (noted briefly in section entitled "General Description of Flight"). The crosshatched portion of the curve was faired in favor of the lift-curve-slope point obtained where the longitudinal oscillation appeared least affected (between 3.53 and 3.6 seconds in fig. 5) by the lateral maneuver.

### Drag

Minimum-drag points given in figure 11(a) were obtained from plots of  $C_D$  against  $C_L$  shown in figure 12. Minimum drag was obtained from the drag polars where an extrapolation of no more than  $0.15C_L$  was involved. The points in figure 12 correspond in respect to Mach number to the  $C_L$  points in figure 9. The low-lift drag information obtained during the lateral maneuver at a Mach number of approximately 1.4 is believed considerably more reliable than stability and lift data obtained at that speed. The longitudinal accelerometer (most important instrument in determining minimum drag) was not affected by roll acceleration, and data of reference 6 indicate very little effect of yaw angle up to  $\pm 6^\circ$  on  $C_D$ . During the flutter phenomena at a Mach number of approximately 1.25 the longitudinal acceleration trace (shown in fig. 6) vibrated only with small amplitude and therefore provided, assuming possible lateral oscillation and model shaking effects were small, what is considered a reasonably accurate indication of minimum drag.

Minimum-drag data from the small-tail models are also given in figure 11(a). Comparison indicates an increase in minimum  $C_D$  due to change to the larger-tail configuration. These drag measurements include the internal drag of the ducts.

The minimum drag of the area-distribution model is presented in figure 11(b) along with the minimum-drag data from the large-tail rocket model. The drag rise obtained on these two models is the same within approximately 10 percent. Similar agreement was obtained between corresponding models of another configuration reported in reference 4. These data indicate that the magnitude of transonic drag rise on a relatively complex airplane configuration may be determined to a first order by means of relatively simple models having the same longitudinal area distribution as the configuration in question. It might be noted that the drag of the rocket model includes internal duct drag. This would affect the comparison of absolute level of drag between the two models and if there were any sudden change in duct drag during the drag rise the comparison of the drag rise magnitude would also be changed somewhat. This latter effect is, however, believed small.

Base pressure measurements were made on this model at the duct exit station by means of orifices located as shown in figure 13(a). One of the orifices was on the plane of symmetry 0.25 inch above the center line of the duct exits, and three manifolded orifices were located around one of the ducts. The variation of the base pressure coefficients  $\Delta p/q$  with Mach number is presented in figure 13(b) along with data previously obtained on a dummy model with no ducts (unpublished data). The center orifice on the dummy model was located the same as in the present test, and the other orifice was located in a position corresponding to the center line of one of the ducts. Comparisons between data from the two models indicate that air flow through the ducts had no effect on the pressure in the center of the base at least at supersonic speeds. Base pressure coefficients obtained from the three manifolded orifices around the duct, however, were more negative (more suction) than at any other point of measurement on either model. Data of reference 12 show this could be mainly due to a jet effect of air flow through the ducts. The top and bottom orifices are, however, also in a position where, as shown in reference 13, the local base pressure could be lowered by proximity of the free airstream. The overall variation of base pressure with Mach number is very similar to that obtained from tests of models with convergent afterbodies reported in references 13 and 14.

The base pressure-drag coefficient of this model (based on wing area) is indicated to be approximately 0.005 between Mach numbers of 1.4 and 1.2 decreasing to approximately zero at Mach number 1.0 and below.

#### Static Longitudinal Stability

Longitudinal pitching period of this model is shown as a function of Mach number in figure 14(a). The scattered points near Mach number 1.4 were obtained, as noted previously, during a combined longitudinal-lateral maneuver. The line faired through the points in figure 14(a) was used along with time-to-damp information to obtain the variation of static stability parameter  $C_{m\alpha}$  with Mach number presented in figure 14(b). The variation of aerodynamic-center position with Mach number as obtained from the  $C_{m\alpha}$  curve of figure 14(b),  $C_{L\alpha}$  curve of figure 10, and the center-of-gravity position ( $0.05\bar{c}$ ) is given in figure 14(c) along with comparable data from the small-tail models.

Qualitatively, aerodynamic-center position shows the same effect of varying Mach number on both large- and small-tail models. The aerodynamic center of the large-tail model is indicated to be rearward of the aerodynamic center of the small-tail models approximately 15 percent  $\bar{c}$  at supersonic and about 7 percent  $\bar{c}$  at subsonic speeds.

When the small-tail model of reference 2 was pulsed to high angles of attack (above the stall) at a Mach number of about 0.7, it became highly unstable. The model of the present test was instrumented with two accelerometers to obtain a measurement of total pitching moment especially in this high angle-of-attack range where large nonlinearities might be expected. Because of a conservative combination of center-of-gravity position and tail settings used in the present test, this model did not reach the high angles encountered in tests of reference 2. There was no evidence, therefore, whether the large-tail model was or was not unstable above the stall.

The pitching-moment data measured by the two accelerometers was of very little value since the model did not reach the lift range where large nonlinearities might be expected and since the buffeting at lift coefficients below the stall precluded measurement of moderate nonlinearities. Therefore, data obtained by this method are not presented in this report.

#### Damping in Pitch

The variation with Mach number of time for pitch oscillations to damp to one-half amplitude is shown in figure 15(a). No value of  $T_{1/2}$  was obtained above Mach number of 1.29 (between 3.5 and 4.3 seconds in fig. 5) because of the large effects of the lateral oscillation on this parameter. A value was not obtained for the oscillation at a Mach number of approximately 0.9 because the trim line was not sufficiently well defined throughout the oscillation.

The damping coefficient  $C_{m_q} + C_{m_{\dot{\alpha}}}$  was obtained from the  $T_{1/2}$  and  $C_{L_{\alpha}}$  information and is presented in figure 15(b) along with the corresponding data from the small-tail models.

The data indicate that  $C_{m_q} + C_{m_{\dot{\alpha}}}$  obtained from the large-tail model is higher than that from the small-tail models except between Mach numbers of 0.8 and 1.1. The difference in variation of damping with Mach number between the two configurations is unexplainable at present.

#### Comparisons

Some of the data from the Ames 6- by 6-foot supersonic tunnel (ref. 8) and the Langley 300 MPH 7- by 10-foot tunnel (ref. 15) can be compared directly with data from the rocket models. Some comparisons are made in figure 16.

In general, the agreement between rocket-model and wind-tunnel data is good. The minimum-drag data from the tests made in the 7- by 10-foot tunnel are not shown because support tare corrections had not been made to these data.

All tests were made with air flow through the ducts. Reynolds number for the rocket-model tests covered the range from  $2.8 \times 10^6$  to  $12 \times 10^6$ . Reynolds numbers for the tests made in the Ames 6- by 6-foot tunnel were  $2.1 \times 10^6$  to  $2.6 \times 10^6$  and for the tests in the Langley 7- by 10-foot tunnel,  $2.23 \times 10^6$ .

#### CONCLUDING REMARKS

A pulsed-control rocket-propelled model of the Douglas X-3 airplane with an enlarged tail of aspect ratio 4.33 has been flown, primarily to provide a comparison of its longitudinal stability, lift, and drag characteristics with those of previously tested models with tails of aspect ratio 3.0.

In general, the tests show that enlarging the tail increased stability, minimum drag, lift-curve slope, and damping (in order of decreasing effect). Comparisons made between rocket-model and wind-tunnel data show good agreement.

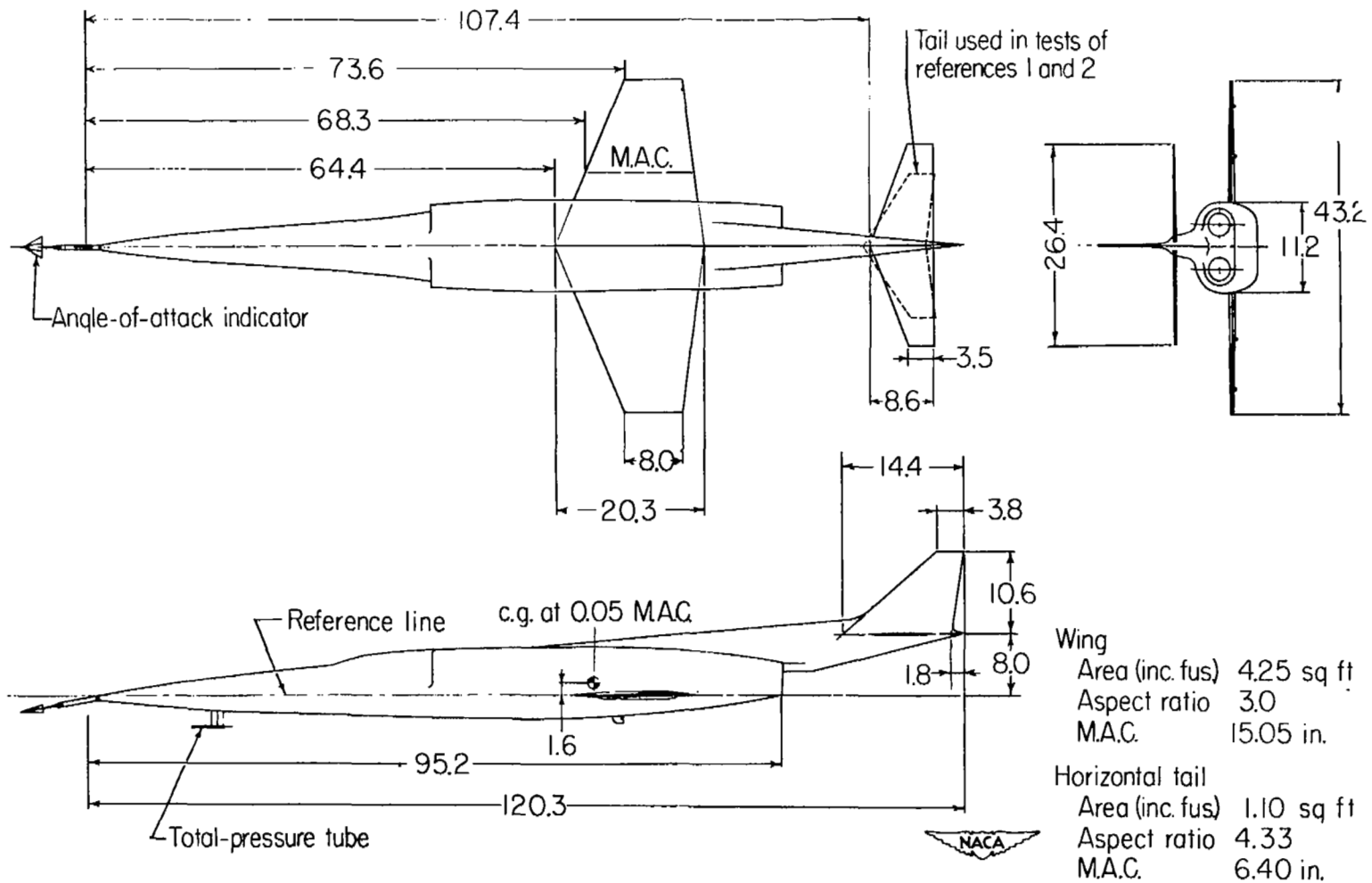
A simple model (finned body of revolution) having the same longitudinal distribution of cross-sectional area as the X-3 airplane-configuration model experienced the same transonic drag rise, within approximately 10 percent.

Langley Aeronautical Laboratory,  
National Advisory Committee for Aeronautics,  
Langley Field, Va., June 9, 1953.

## REFERENCES

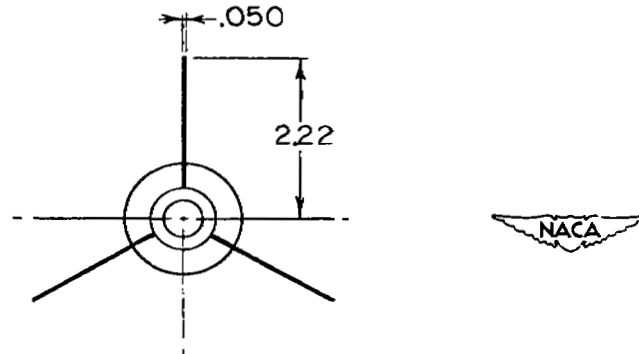
1. Mitchell, Jesse L., and Peck, Robert F.: An Investigation of the Longitudinal Characteristics of the X-3 Configuration Using Rocket-Propelled Models. Preliminary Results at Mach Numbers From 0.65 to 1.25. NACA RM L50J03, 1950.
2. Peck, Robert F., and Mitchell, Jesse L.: An Investigation of the Longitudinal Characteristics of the X-3 Configuration With Wing and Horizontal Tail Surfaces of Aspect Ratio 3.0 by Means of Rocket-Propelled Models. Results at High Lift Coefficients. NACA RM L51G10, 1951.
3. Whitcomb, Richard T.: A Study of the Zero-Lift Drag-Rise Characteristics of Wing-Body Combinations Near the Speed of Sound. NACA RM L52H08, 1952.
4. Hopko, Russell N., Piland, Robert O., and Hall, James R.: Drag Measurements at Low Lift of a Four-Nacelle Airplane Configuration Having a Longitudinal Distribution of Cross-Sectional Area Conducive to Low Transonic Drag Rise. NACA RM L53E29, 1953.
5. Gillis, Clarence L., Peck, Robert F., and Vitale, A. James: Preliminary Results From a Free-Flight Investigation at Transonic and Supersonic Speeds of the Longitudinal Stability and Control Characteristics of an Airplane Configuration With a Thin Straight Wing of Aspect Ratio 3. NACA RM L9K25a, 1950.
6. Mitcham, Grady L., and Blanchard, Willard S., Jr.: Low-Lift Drag and Stability Data From Rocket Models of a Modified-Delta-Wing Airplane With and Without External Stores at Mach Numbers From 0.8 to 1.36. NACA RM L53A27, 1953.
7. Mitchell, Jesse L., and Peck, Robert F.: An NACA Vane-Type Angle-of-Attack Indicator for Use at Subsonic and Supersonic Speeds. NACA RM L9F28a, 1949.
8. Olson, Robert N., and Chubb, Robert S.: Wind-Tunnel Tests of a 1/12-Scale Model of the X-3 Airplane at Subsonic and Supersonic Speeds. NACA RM A51F12, 1951.
9. Chapman, Rowe, Jr., and Morrow, John D.: Longitudinal Stability and Drag Characteristics at Mach Numbers From 0.70 to 1.37 of Rocket-Propelled Models Having a Modified Triangular Wing. NACA RM L52A31, 1952.

10. Vitale, A. James, McFall, John C., Jr., and Morrow, John D.: Longitudinal Stability and Drag Characteristics at Mach Numbers From 0.75 to 1.5 of an Airplane Configuration Having a  $60^\circ$  Swept Wing of Aspect Ratio 2.24 As Obtained From Rocket-Propelled Models. NACA RM L51K06, 1952.
11. Gillis, Clarence L.: Buffeting Information Obtained From Rocket-Propelled Airplane Models Having Thin Unswept Wings. NACA RM L50H22a, 1950.
12. Cortright, Edgar M., Jr., and Schroeder, Albert H.: Investigation at Mach Number 1.91 of Side and Base Pressure Distributions Over Conical Boattails Without and With Jet Flow Issuing From Base. NACA RM E51F26, 1951.
13. Peck, Robert F.: Flight Measurements of Base Pressure on Bodies of Revolution With and Without Simulated Rocket Chambers. NACA RM L50I28a, 1950.
14. Katz, Ellis R., and Stoney, William E., Jr.: Base Pressures Measured on Several Parabolic-Arc Bodies of Revolution in Free Flight at Mach Numbers From 0.8 to 1.4 and at Large Reynolds Numbers. NACA RM L51F29, 1951.
15. McKee, John W., and Riebe, John M.: An Investigation of a 0.16-Scale Model of the Douglas X-3 Airplane To Determine Means of Improving the Low-Speed Longitudinal Stability and Control Characteristics. NACA RM L52H01, 1952.



(a) Rocket-propelled Douglas X-3 airplane-configuration model.

Figure 1.- Sketches of test models. All dimensions are in inches.



(b) Helium-gun model having same longitudinal distribution of cross-sectional area as X-3 airplane-configuration model.

Figure 1.- Concluded.

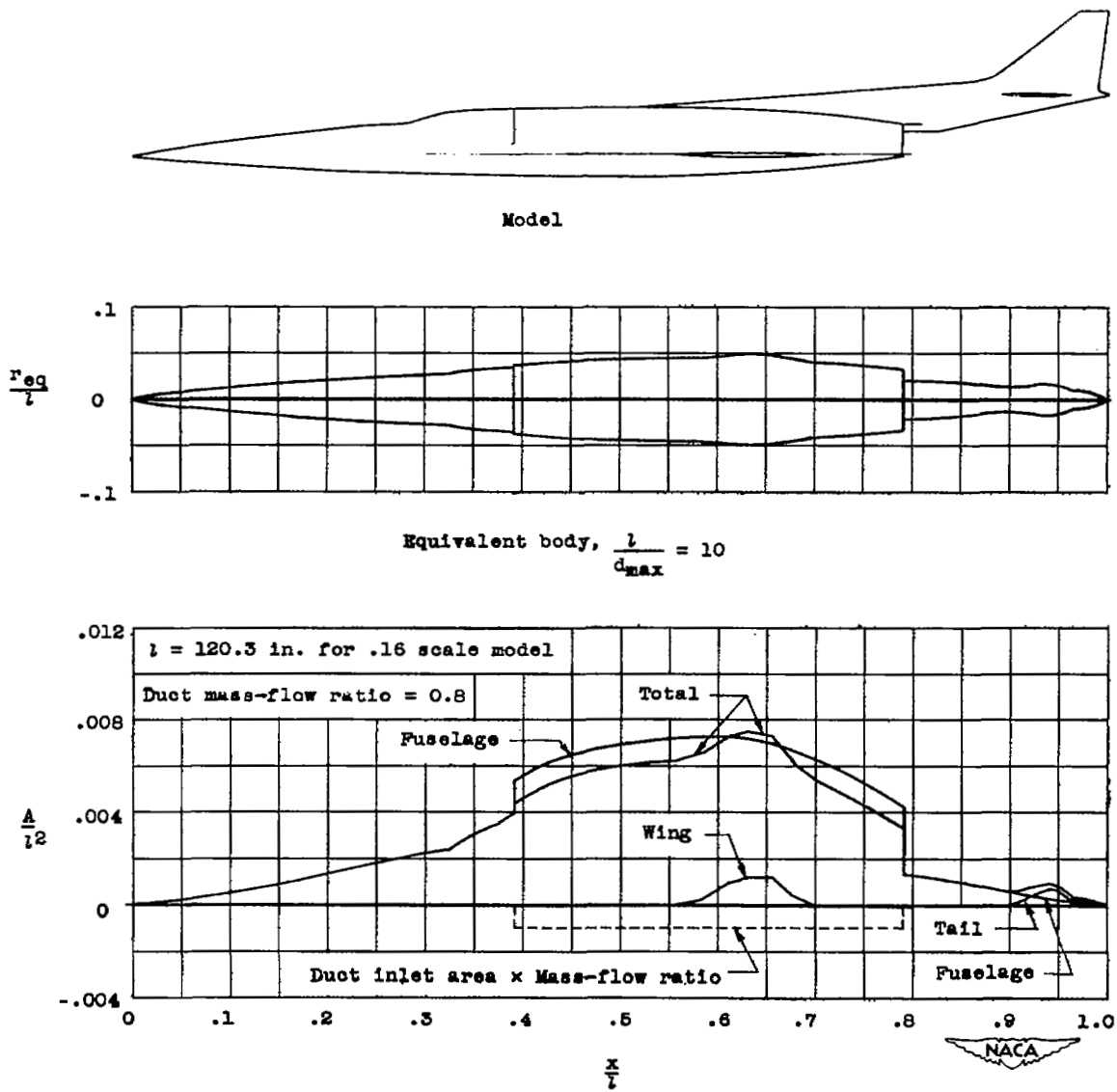
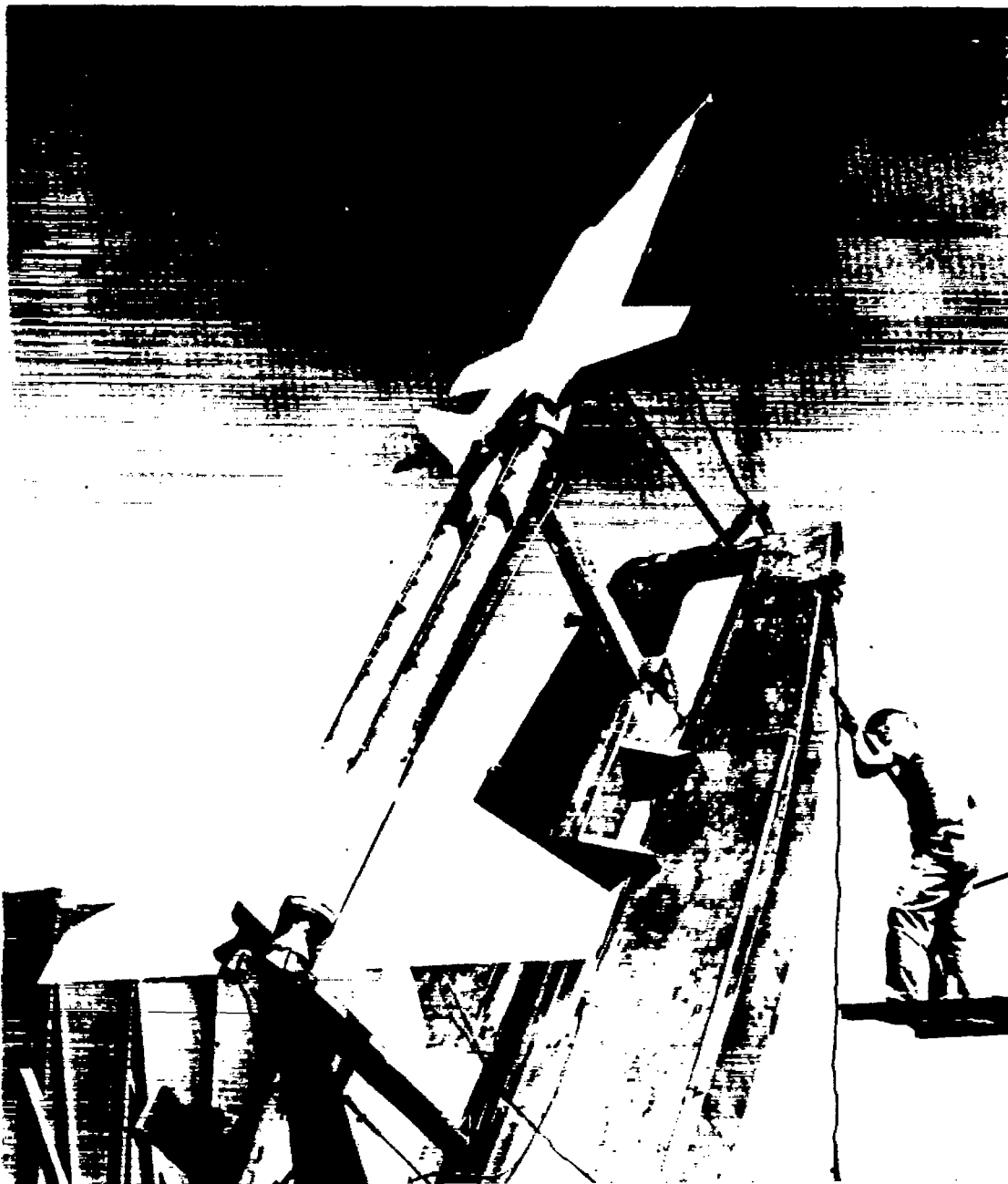


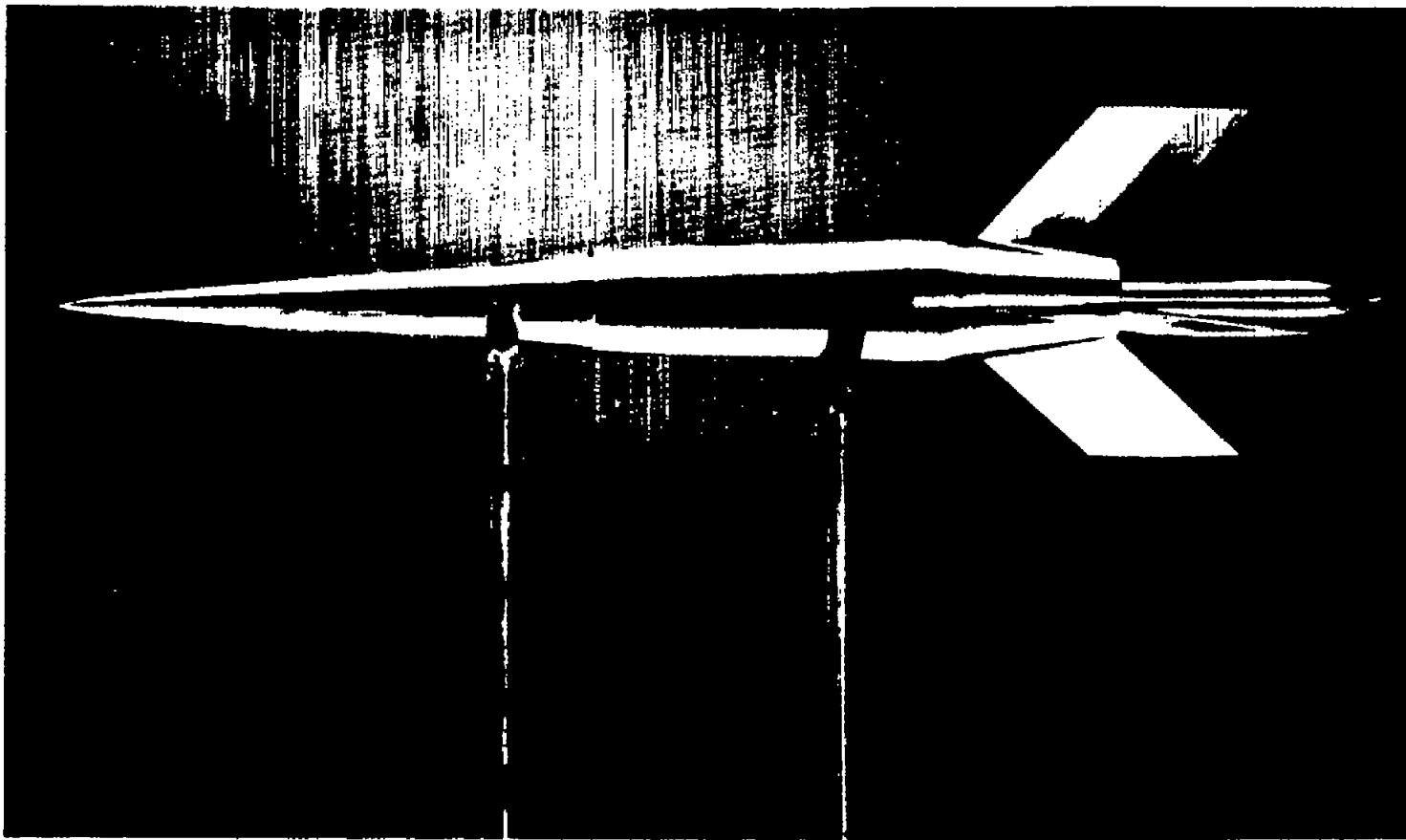
Figure 2.- Cross-sectional-area distribution and equivalent round body.



L-75938.1

(a) Rocket-propelled airplane-configuration model and booster on launcher.

Figure 3.- Photographs of models.



L-79809

(b) Helium-gun model having same longitudinal distribution of cross-sectional area as airplane-configuration model.

Figure 3.- Concluded.

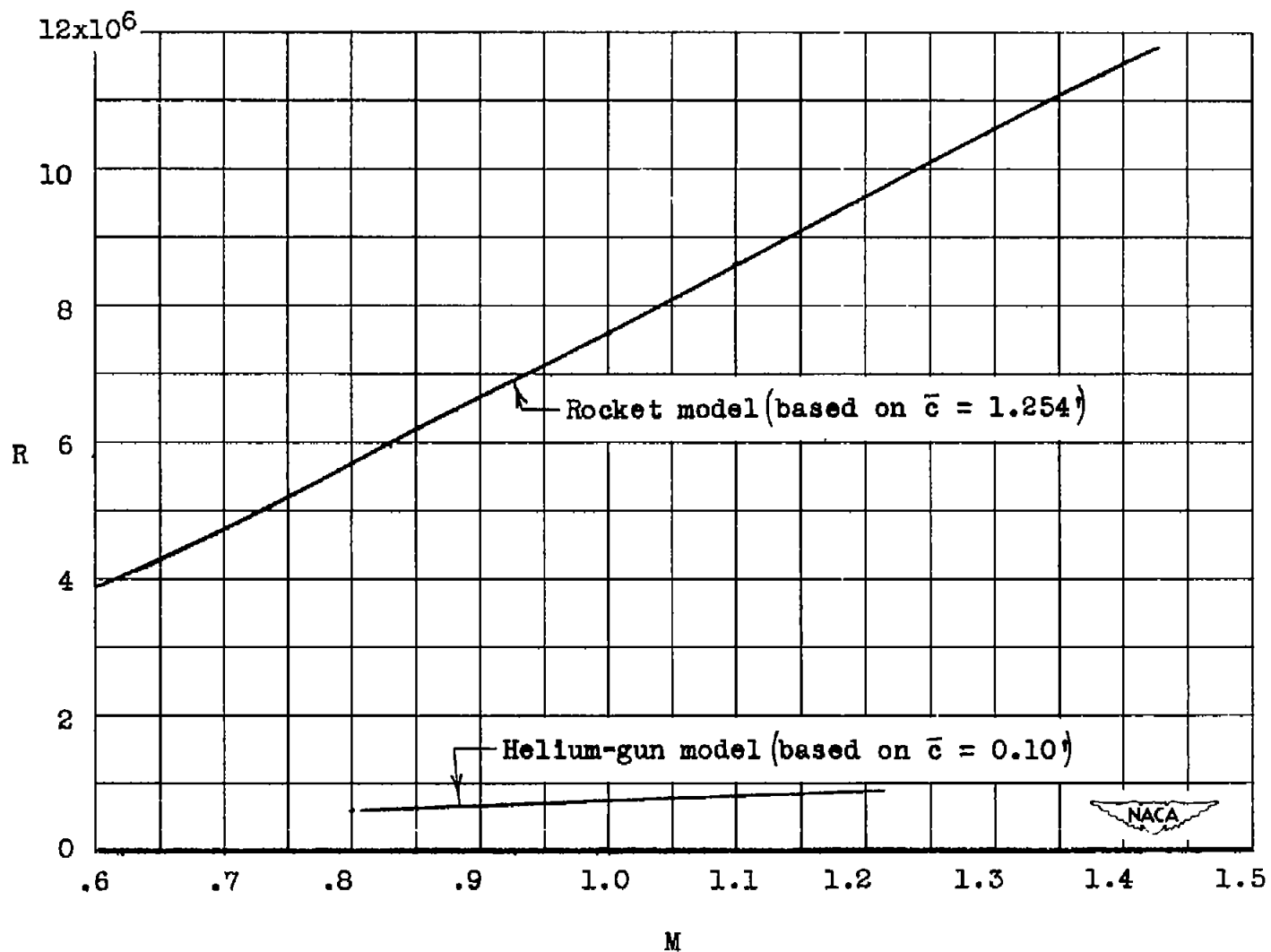


Figure 4.- Test Reynolds number based on wing mean aerodynamic chord.

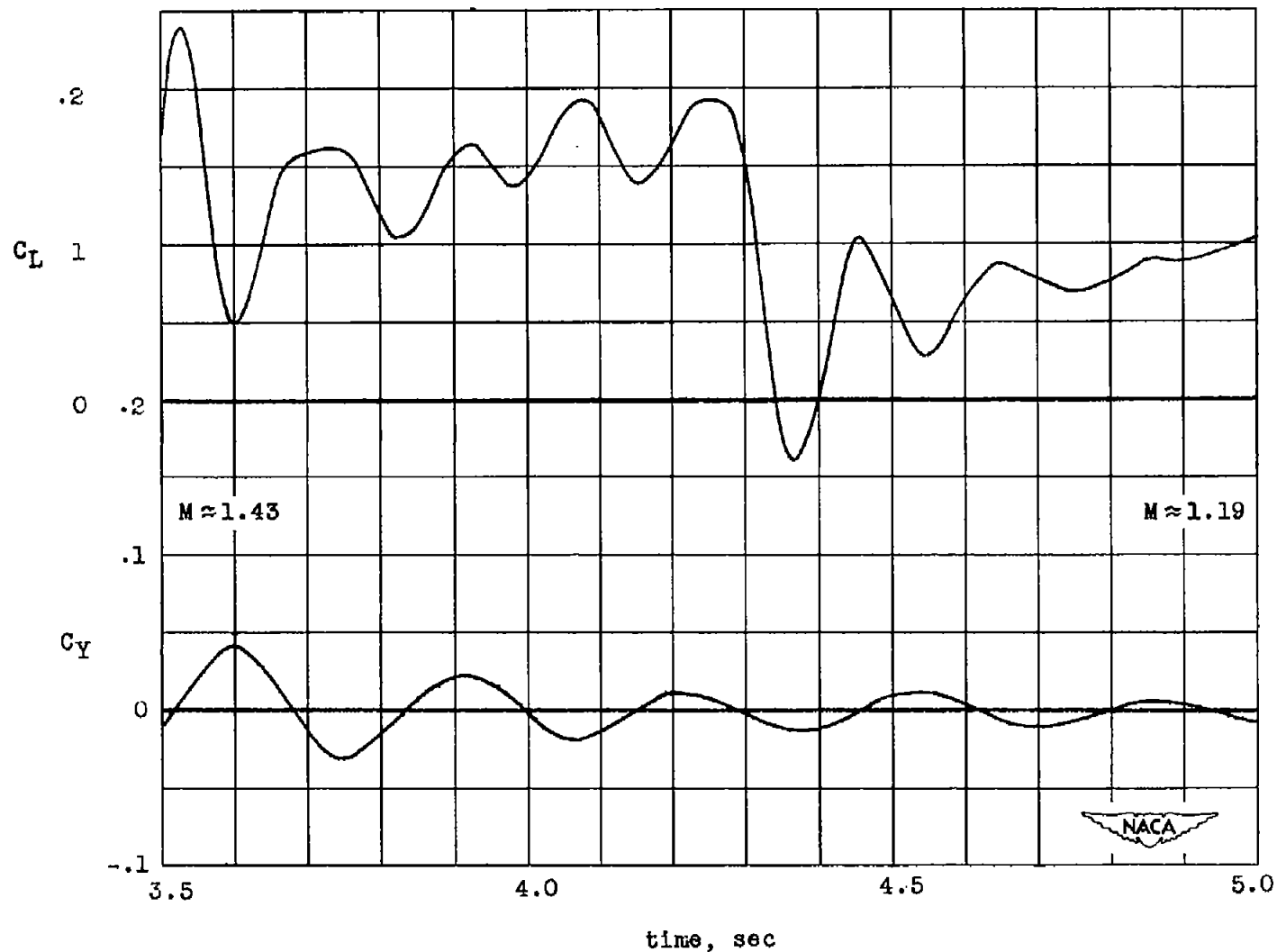


Figure 5.- Variation of lift and side-force coefficients with time during lateral oscillation induced at model-booster separation.

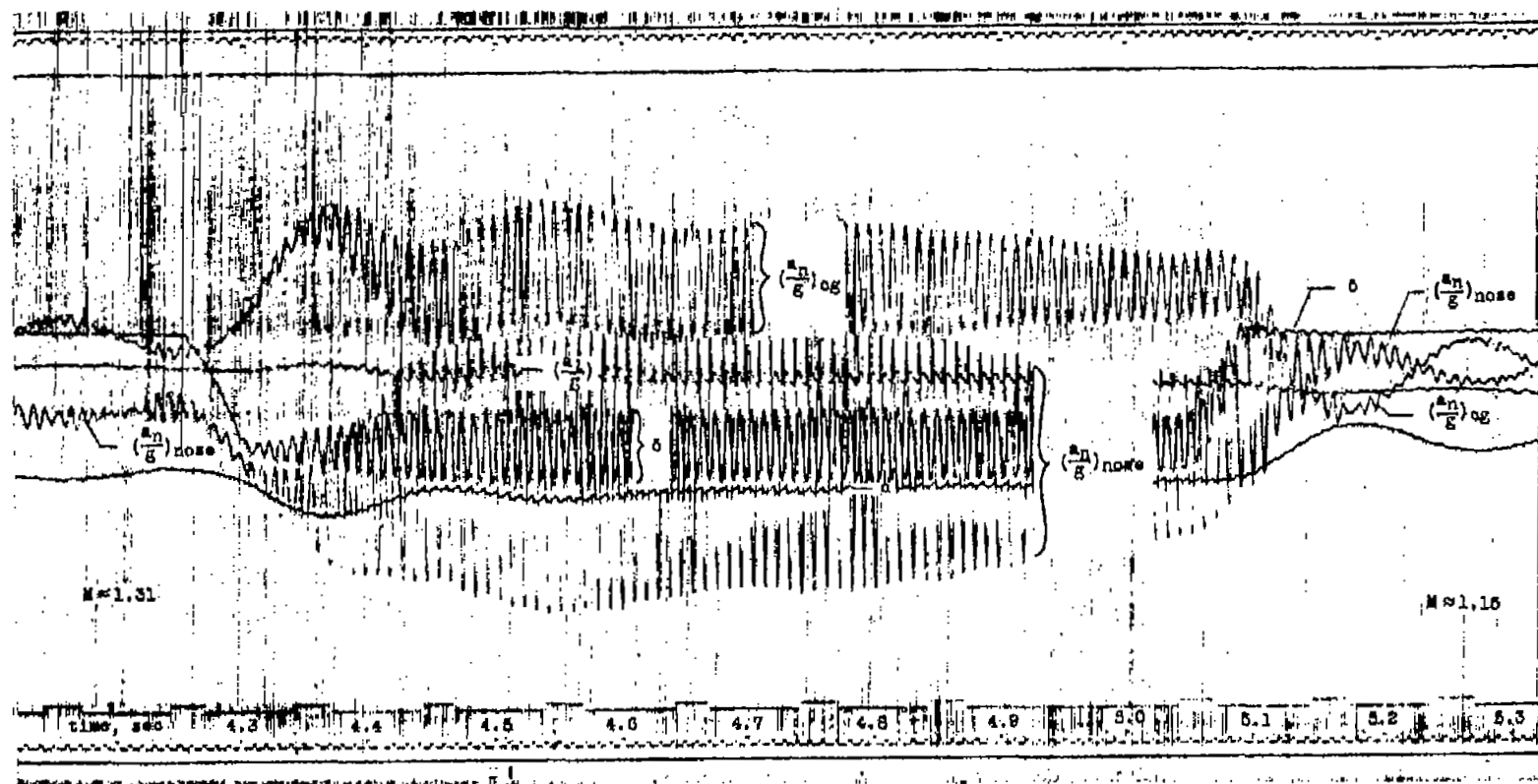
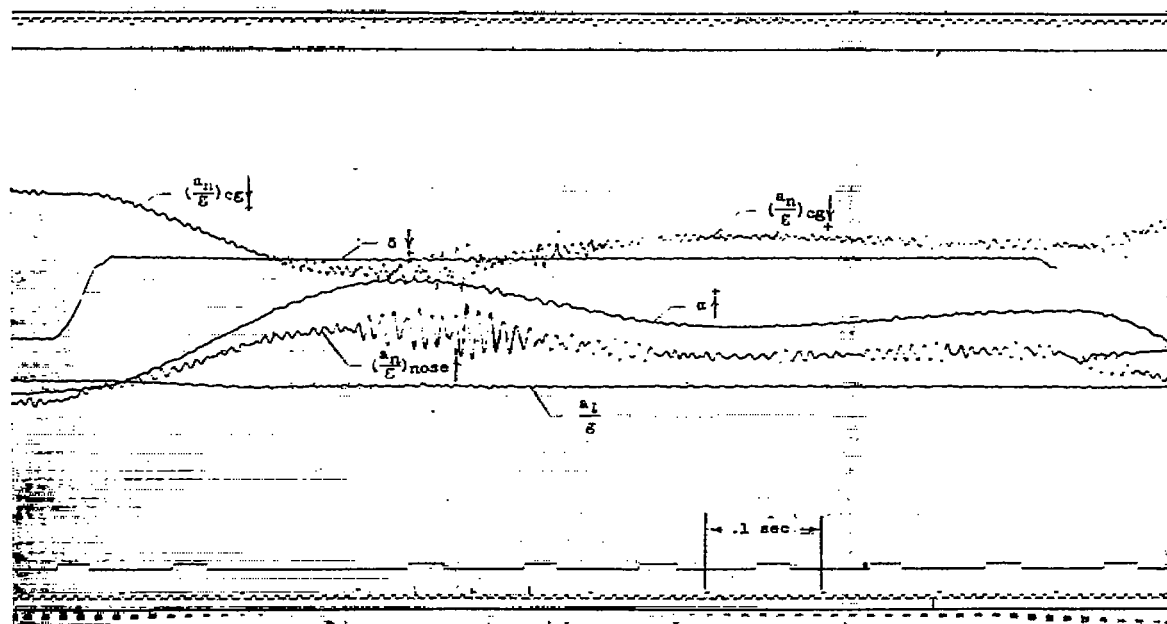
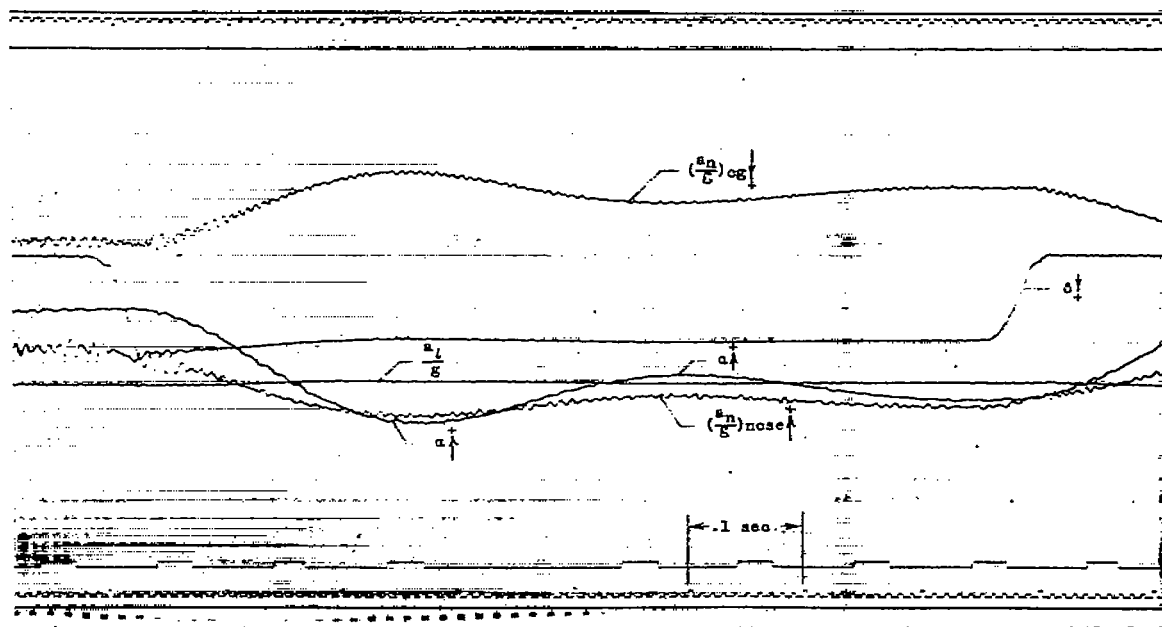


Figure 6.- Portion of telemeter record taken during flutter.



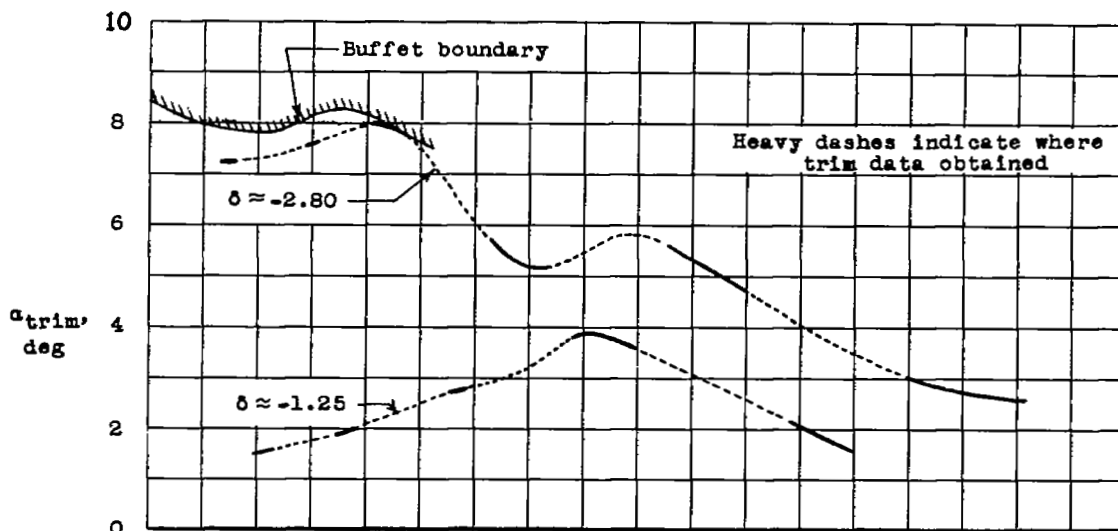


(a) During buffeting.

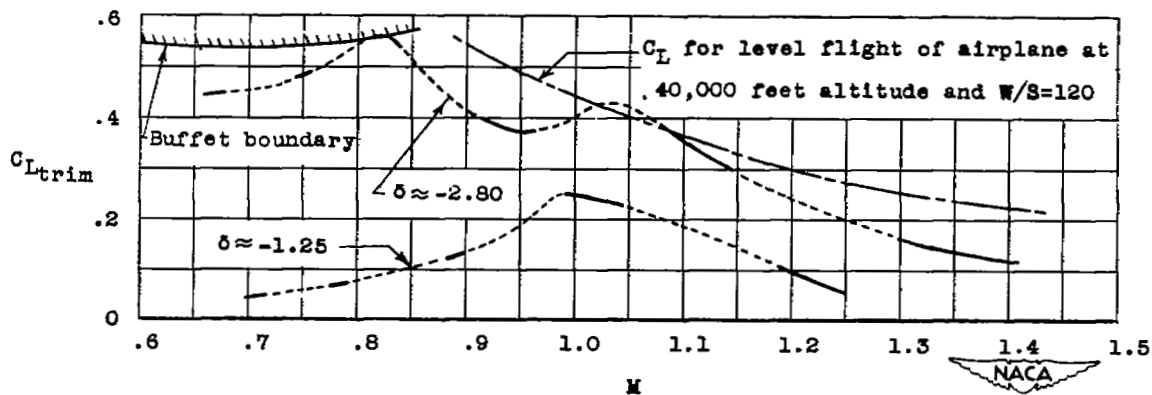


(b) Without buffeting.

Figure 7.- Typical portions of telemeter record with and without buffeting.

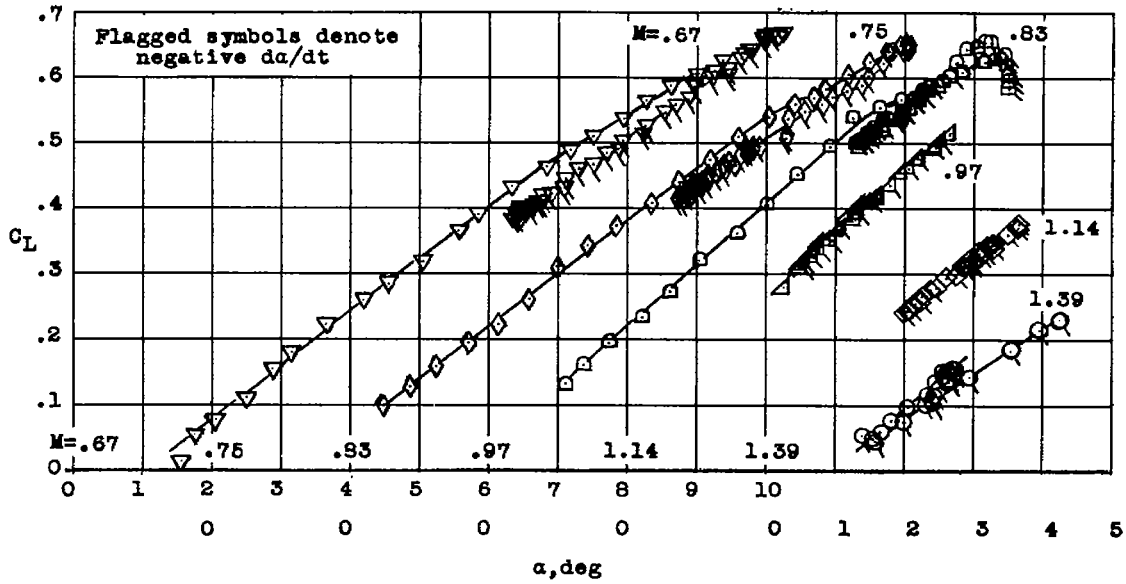


(a) Angle of attack.

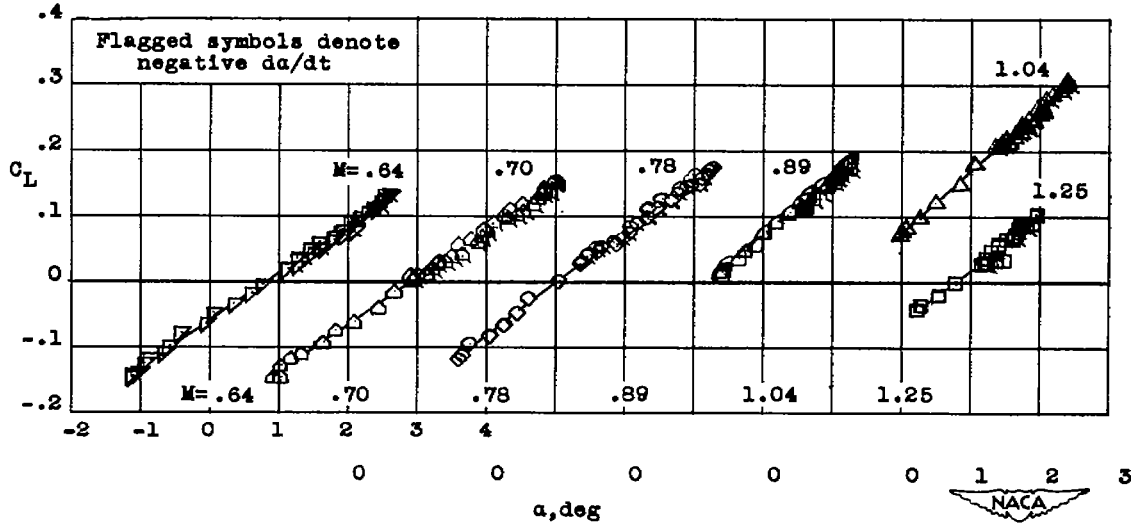


(b) Trim lift coefficient.

Figure 8.- Trim characteristics and buffet boundaries. Center of gravity at 5 percent mean aerodynamic chord.



(a)  $\delta \approx -2.80$ .



(b)  $\delta \approx -1.25$ .

Figure 9.- Variation of lift coefficient with angle of attack.

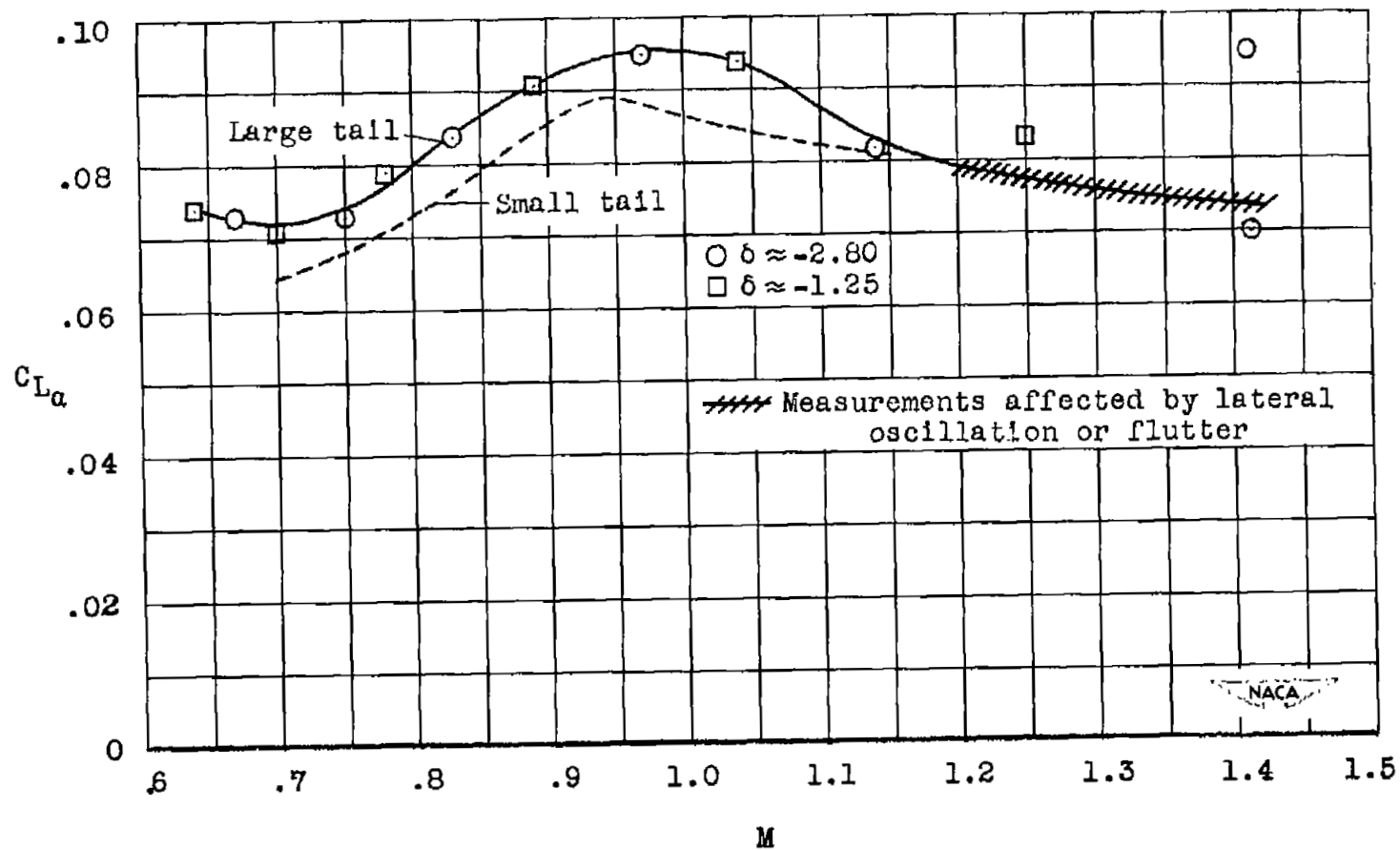
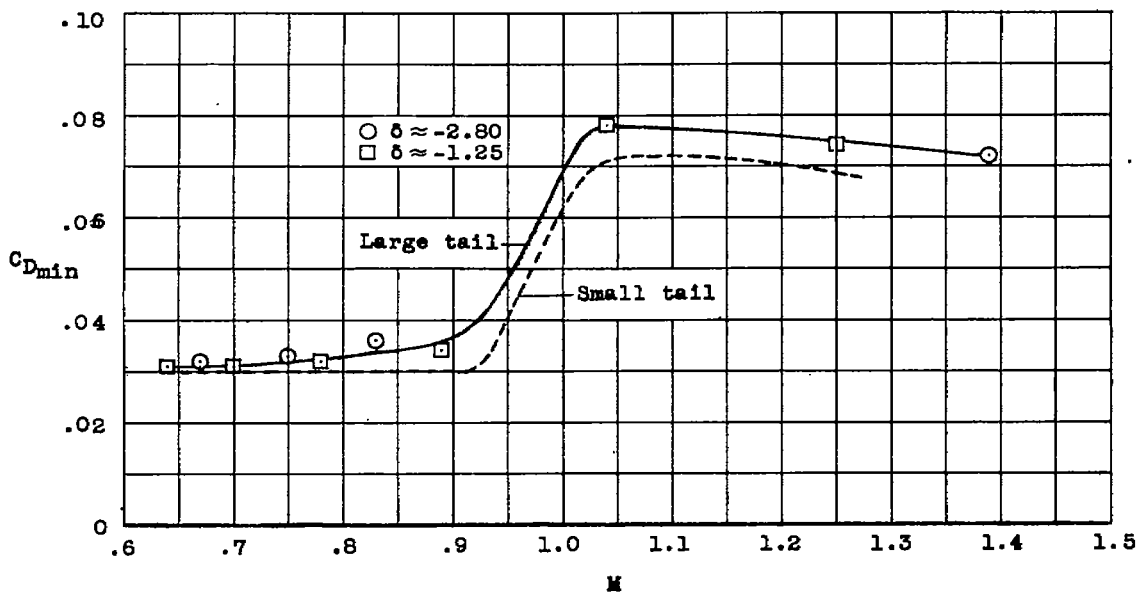
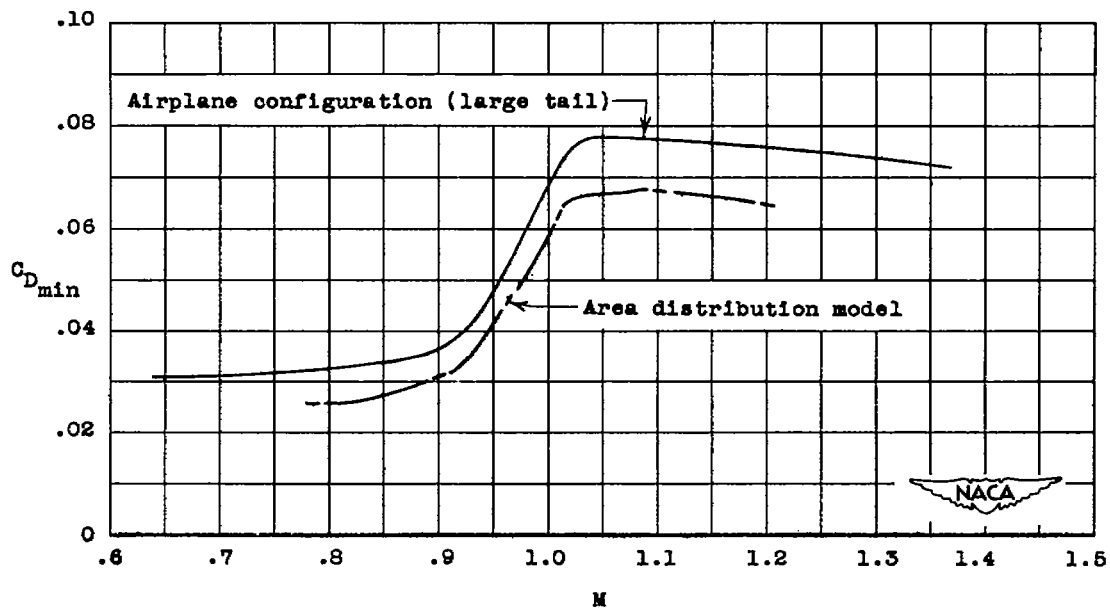


Figure 10.- Lift-curve slopes.



(a) Airplane configurations.



(b) Airplane-configuration and area-distribution models.

Figure 11.- Variation of minimum drag coefficients with Mach number.

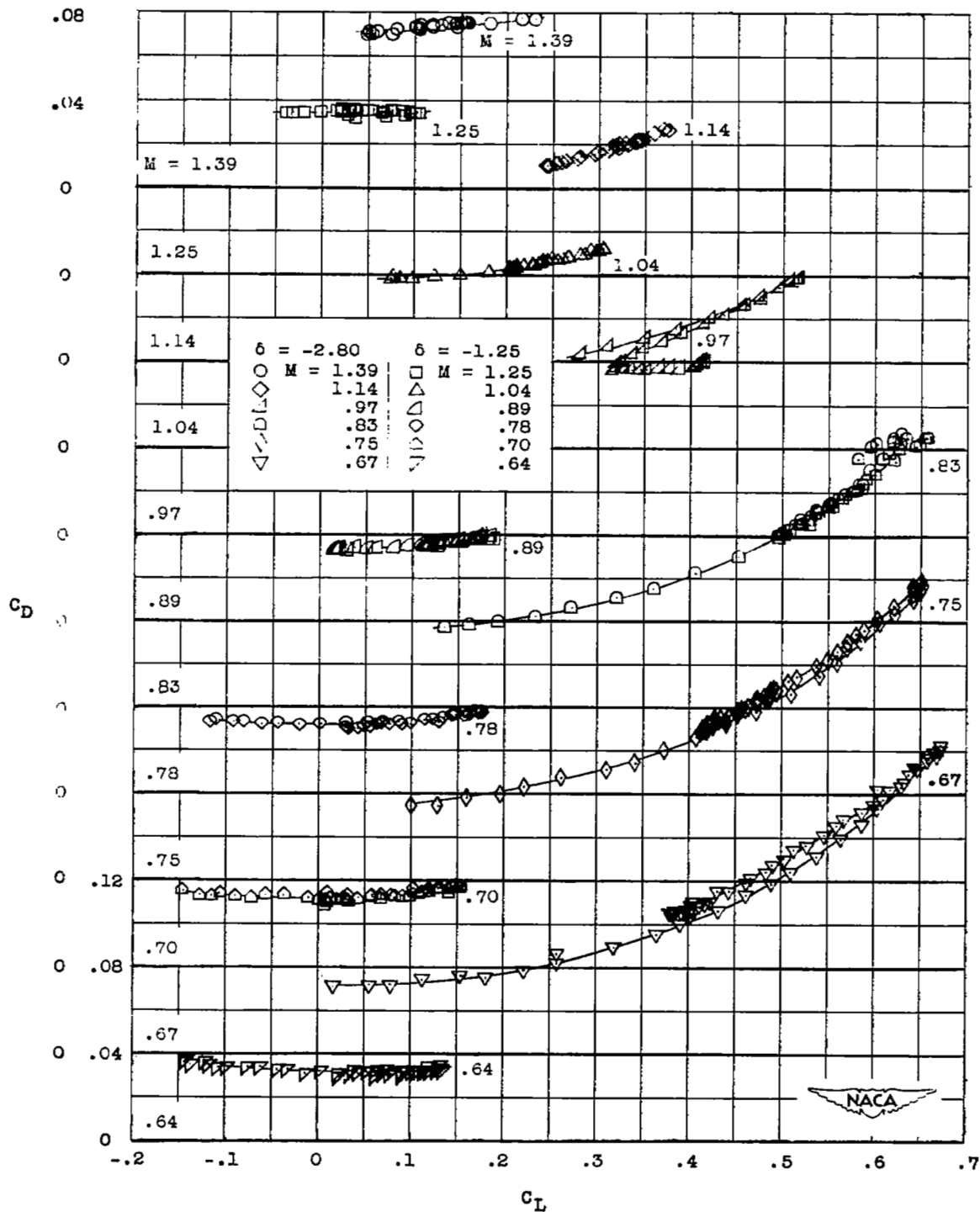
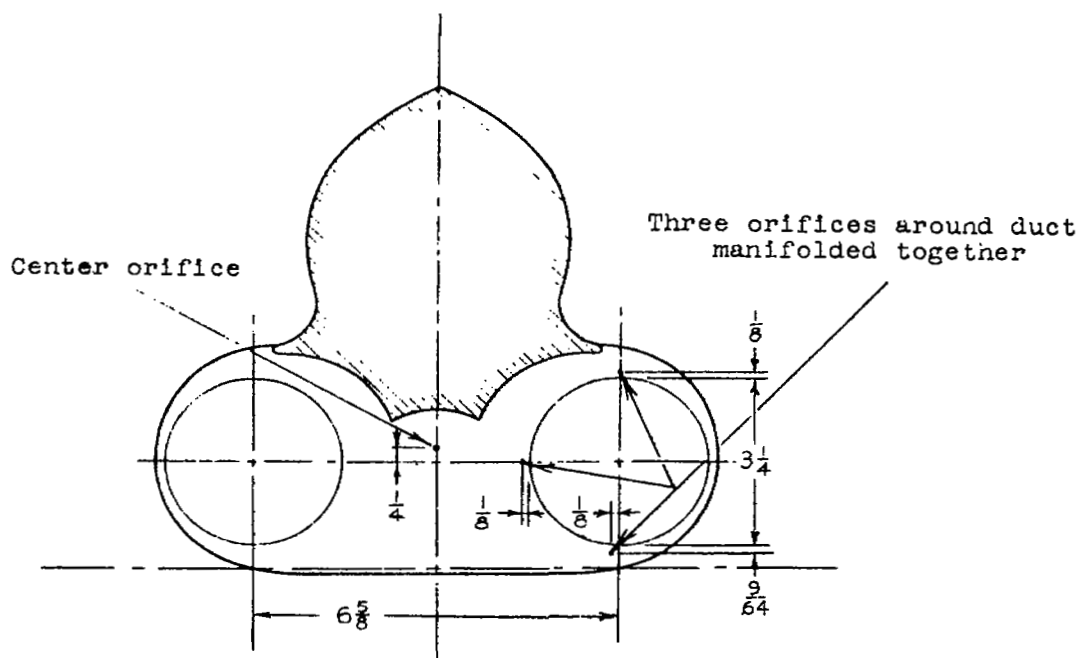
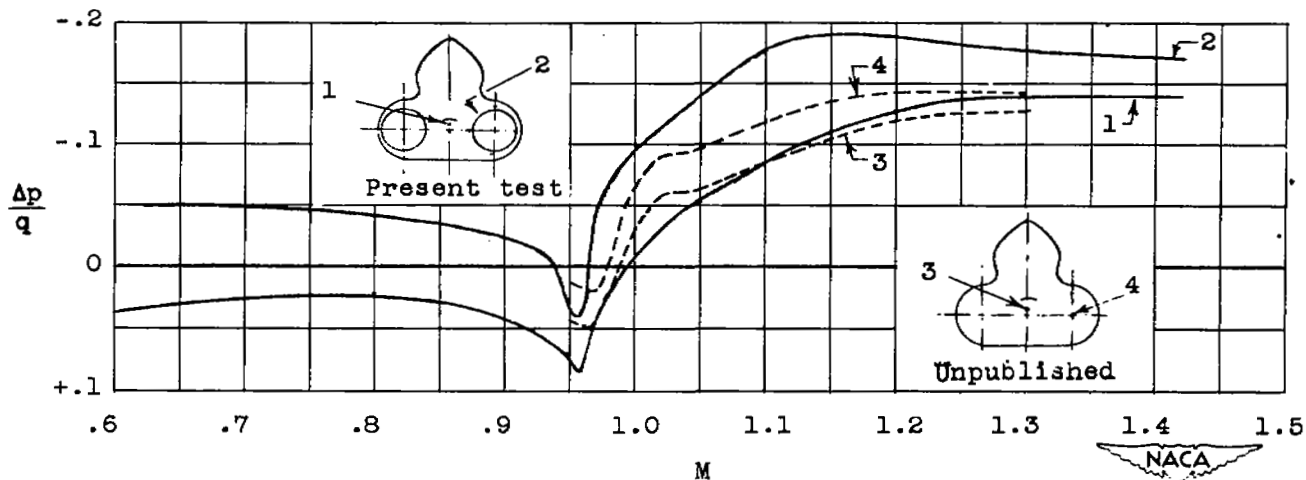


Figure 12.- Variation of drag coefficient with lift coefficient.

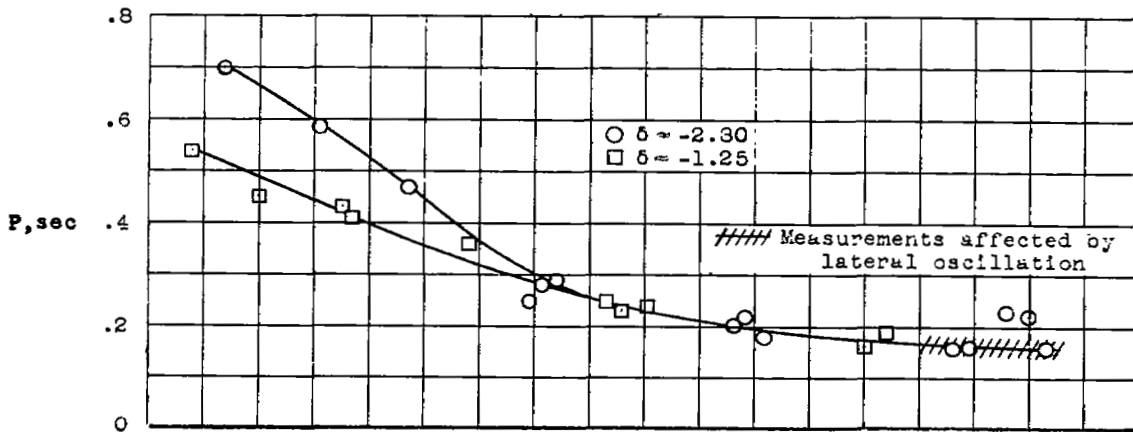


(a) Location of base-pressure orifices at exit station of ducts.

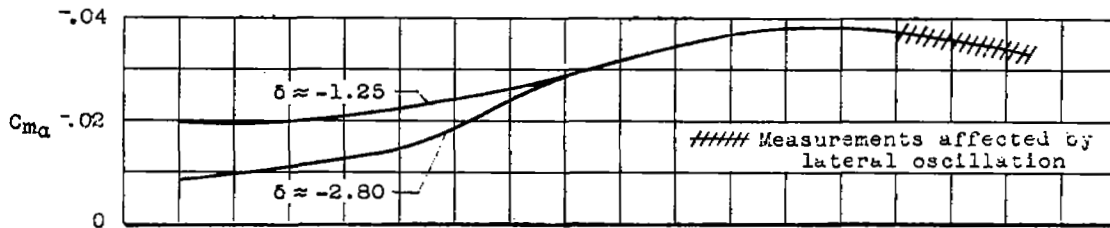


(b) Variation of base-pressure coefficients with Mach number from models with and without ducts.

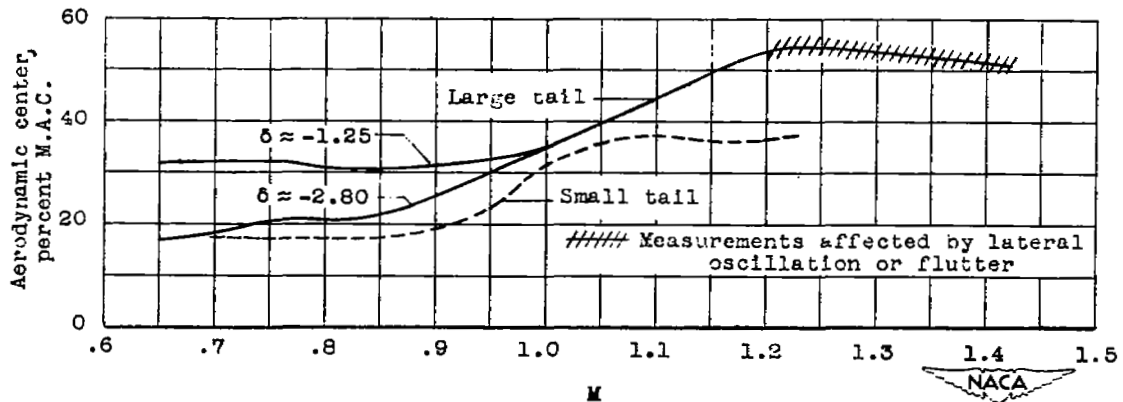
Figure 13.- Base-pressure information.



(a) Period of oscillations.

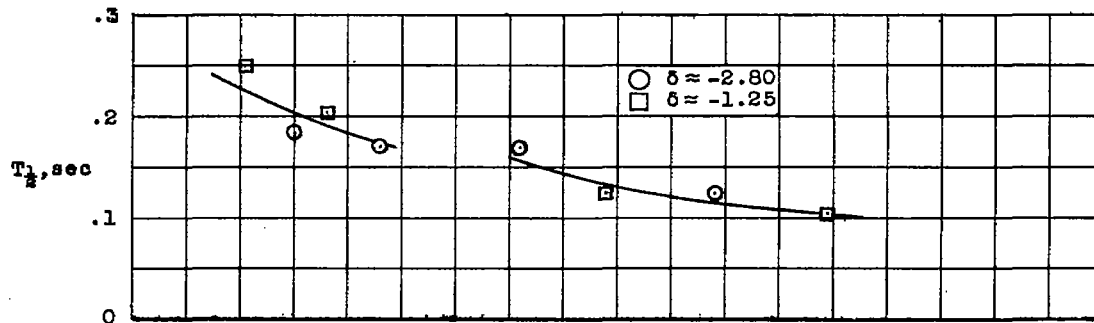


(b) Static stability.

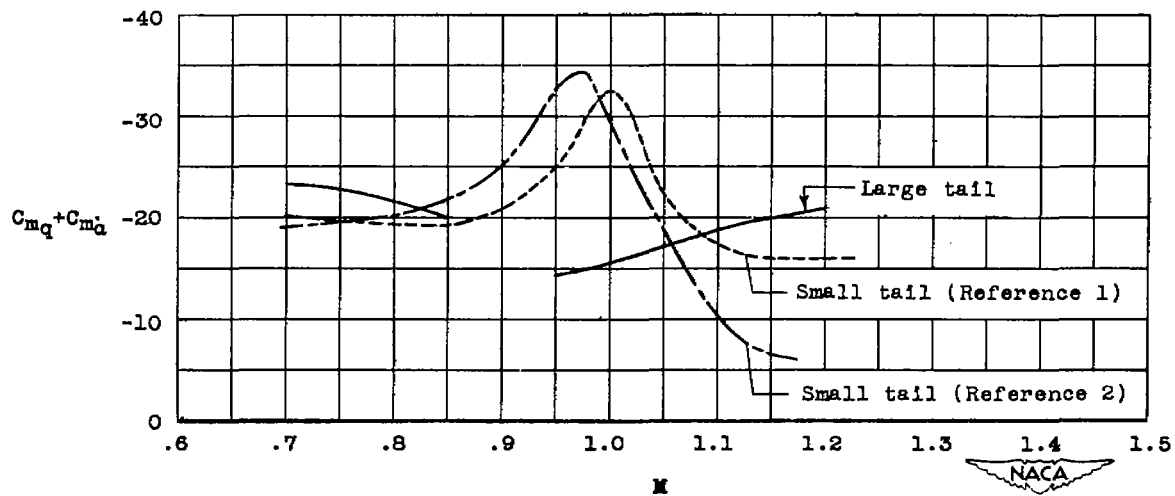


(c) Aerodynamic-center location.

Figure 14.- Static longitudinal stability characteristics. Center of gravity at 5 percent mean aerodynamic chord.

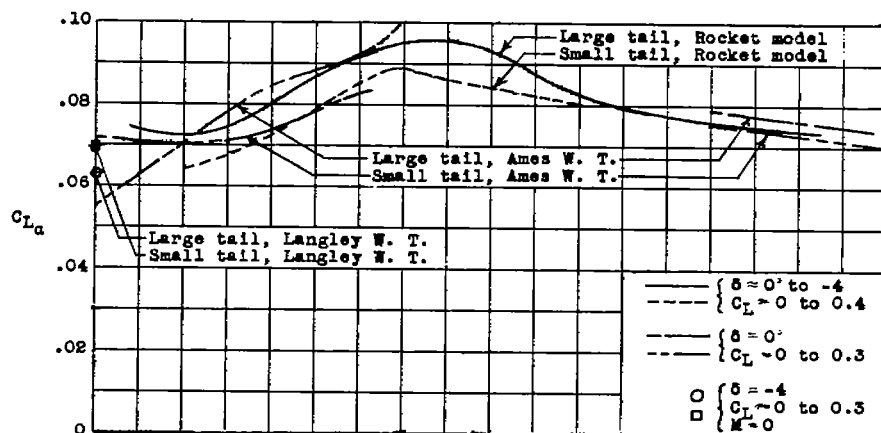


(a) Time to damp to one-half amplitude.

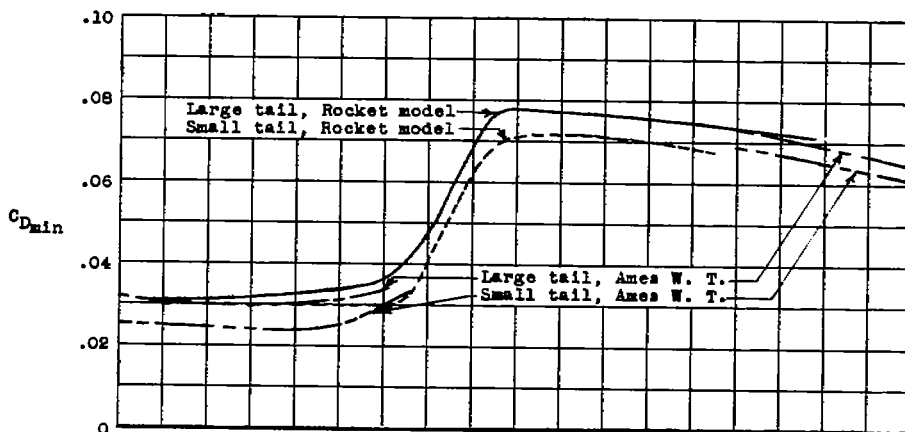


(b) Damping derivative.

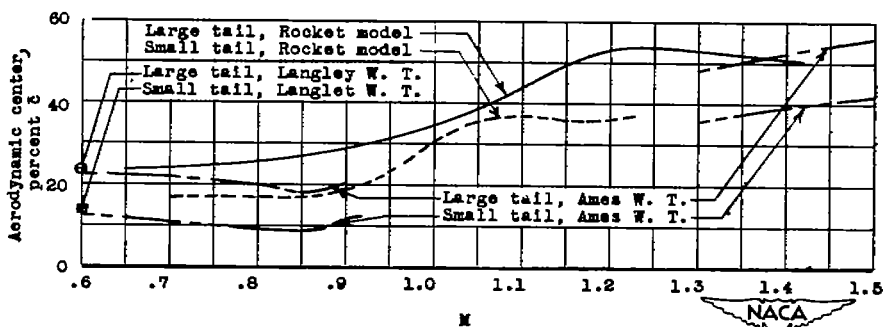
Figure 15.- Damping characteristics of longitudinal short-period oscillation.



(a) Lift-curve slope.



(b) Minimum drag.



(c) Aerodynamic center.

Figure 16.- Comparisons of data from rocket and wind-tunnel models of X-3 configurations with large and small tails.

SECURITY INFORMATION

~~CONFIDENTIAL~~

NASA Technical Library



3 1176 01437 1190

~~CONFIDENTIAL~~